Fully Nonlinear Edge Gyrokinetic Simulations of Kinetic Geodesic-Acoustic Modes and Boundary Flows[1]

X. Q. Xu[1], E. Belli[2], K. Bodi[3], J. Candy[2], C. S. Chang[4], B. I. Cohen[1], R. H. Cohen[1], P. Colella[5] A. M. Dimits[1], M. R. Dorr[1], Z. Gao[6], J. A. Hittinger[1], S. Ko[7], S. Krasheninnikov[3], G. R. McKee[8], W. M. Nevins[1], T. D. Rognlien[1], P. B. Snyder[2], J. Suh[7], M. V. Umansky[1]

1) Lawrence Livermore National Laboratory, Livermore, CA 94550 USA,
2) General Atomics, San Diego, CA 92186 USA
3) University of California, San Diego, La Jolla, CA 92093 USA
4) Courant Institute of Mathematical Sciences, New York University, NY, NY 10012
5) Lawrence Berkeley National Laboratory, Berkeley, CA 94720 USA
6) Department of Engineering Physics, Tsinghua University, Beijing, P. R. China
7) Korea Advanced Institute of Science and Technology, Daejeon, R. Korea
8) University of Wisconsin-Madison, Madison, Wisconsin 53706, USA

e-mail contact of main author: xxu@llnl.gov

Abstract. We present edge gyrokinetic neoclassical simulations of tokamak plasmas using the fully non-linear (full-f) continuum code TEMPEST. A nonlinear Boltzmann model is used for the electrons. The electric field is obtained by solving the 2D gyrokinetic Poisson Equation. We demonstrate the following: (1) High harmonic resonances ($n > 2$) significantly enhance geodesic-acoustic mode (GAM) damping at high-q (tokamak safety factor), and are necessary to explain the damping observed in our TEMPEST q-scans and consistent with the experimental measurements of the scaling of the GAM amplitude with edge q_{95} in the absence of obvious evidence that there is a strong q dependence of the turbulent drive and damping of the GAM. (2) The kinetic GAM exists in the edge for steep density and temperature gradients in the form of outgoing waves, its radial scale is set by the ion temperature profile, and ion temperature inhomogeneity is necessary for GAM radial propagation. (3) The development of the neoclassical electric field evolves through different phases of relaxation, including GAMs, their radial propagation, and their long-time collisional decay. (4) Natural consequences of orbits in the pedestal and scrape-off layer region in divertor geometry are substantial non-Maxwellian ion distributions and flow characteristics qualitatively like those observed in experiments.

1. Introduction

Geodesic acoustic modes (GAMs) have been clearly identified experimentally in tokamak and stellarator plasmas and play an important role in edge transport barrier formation. Both the GAM and zonal flows (ZF) are driven by turbulence, however the GAM can be damped both by wave-particle resonances and collisions, while gyrokinetic ZFs are only damped by the collisional friction between trapped and circulating ions. The turbulence fluctuation levels and transport are in turn regulated by the GAM and ZFs via the time-varying ExB flow shear de-correlation, which impact on the L-H transition. This work presents several important advances in our understanding of GAMs and zonal flow, and radial electric field of a neoclassical plasma.

2.   A heuristic kinetic model for the evolution of radial electric field in toroidal plasmas

In the long wavelength limit $k_\perp \rho_\alpha \ll 1$, the self-consistent electric field is computed from the full-f gyrokinetic Poisson equation for multiple species [1, 2]

$$\sum_\alpha \frac{\rho_\alpha^2}{2\lambda_{D\alpha}^2} \nabla_\perp \cdot (N_\alpha \nabla_\perp \Phi) + \nabla^2 \Phi = -4\pi e \left[\sum_\alpha Z_\alpha N_\alpha(\mathbf{x}, t) - n_e(\mathbf{x}, t) \right] \qquad (1)$$

It can be shown that by taking the time derivative and flux-surface averaging Eq. (1), assuming the electrostatic potential to be constant within a flux surface, substituting the 0th-moment of the conservative form of gyrokinetic equation for the density on the right side, and finally integrating Eq. (1) over the radial coordinate (valid for a local analysis) with $E_r = 0$ at the boundaries, the radial electric field evolution obeys the radial Ampére-Maxwell law averaged over a closed-flux surface

$$\left(1 + \sum_\alpha \frac{c^2}{v_{A\alpha}^2}\right) \frac{\partial}{\partial t} \langle \mathbf{E} \cdot \nabla \psi \rangle = -4\pi \sum_\alpha \langle \mathbf{J} \cdot \nabla \psi \rangle = -\sum_\alpha \frac{4\pi Z_\alpha e}{M_\alpha} \langle \int B_\parallel^* d\bar{v}_\parallel d\bar{\mu} F_\alpha \bar{\mathbf{v}}_d \cdot \nabla \psi \rangle \quad (2)$$

where ψ is the poloidal magnetic flux, $\langle \cdots \rangle$ represents the flux surface average, and $\mathbf{J}$ is the sum of all the current in the plasma, including the gyro-viscosity current, and the ion guiding-center current due to its orbital dynamics (the corresponding electron current is typically neglected in tokamak geometry, because it is smaller than the ion current by a factor of the mass ratio m_e/m_i). The quasi-steady-state radial electric field E_r on a magnetic surface is obtained from the condition $\langle j_\psi \rangle = 0$. We note the mathematical equivalence of the two approaches for solving the radial electric field of a neoclassical plasma from Eq. (1) and Eq. (2) in the large-aspect-ratio limit.

By taking the time derivative of Eq. (2), inserting gyrokinetic equation into the right side, and then assuming $F_\alpha \simeq F_{M\alpha} + \delta f_\alpha$ in the integral, where $F_{M\alpha}$ is the local Maxwellian distribution function (for simplicity assuming isothermality; the inclusion of an ion temperature gradient leads to more complicated neoclassical sources, but with precisely the same final conclusion except for the appearance of E_r^{neo}), we obtain a dynamical equation for the radial electric field,

$$\left(1 + \sum_\alpha \frac{c^2}{v_{A\alpha}^2}\right) \frac{\partial^2}{\partial t^2} E_r + \sum_\alpha \frac{4\pi Z_\alpha^2 e^2}{T_\alpha} \langle \int d^3 v F_M v_{dr}^2 \rangle E_r$$

$$- \quad 4\pi e \sum_\alpha Z_\alpha \langle \int d^3 v v_{dr} (\mathbf{v}_\parallel + \mathbf{v}_{d\alpha}) \cdot \nabla \delta f_\alpha \rangle + 4\pi e \sum_\alpha Z_\alpha \langle \int d^3 v v_{dr} C(\delta f_\alpha) \rangle$$

$$= \quad \sum_\alpha 4\pi Z_\alpha e \langle \int d^3 v F_M v_{dr}^2 \rangle \frac{d \ln N_\alpha}{dr}. \qquad (3)$$

where the first of group terms on the left side represents the displacement current and ion polarization currents, the second term gives the GAM frequency, the third term yields the GAM collisionless damping, and the fourth term produces the collisional damping ($C(\delta f)$ is the linearized ion collision operator). In the quasi-steady state with a drifting Maxwellian distribution $\delta f_\alpha \propto v_\parallel F_{M\alpha}$, the last term on the right side furnishes the source for the standard neoclassical relationship between E_r from the second term and the parallel flow $U_\parallel$ from streaming in the third term on the left side. Here $E_r = \mathbf{E} \cdot \nabla \psi$. The solution to this

equation describes relaxation of the radial electric field and, heuristically, can be written in the form:

$$E_r(t) = E_r^{neo} + \left[E_r^{HR} + E_r^{GAM} e^{-(i\omega_{GAM} + \gamma_{GAM})t} \right] e^{-\gamma_c t}. \tag{4}$$

where (see Sec.3.) $\omega_{GAM} = (\sqrt{7 + 4\tau}/2)(v_{Ti}/R)$ is the GAM frequency [3], $\tau = T_e/T_i$ for a single ion species and R is the major radius, where γ_{GAM} is the collisionless GAM damping [4, 5, 6, 7, 8], $E_r^{RH}(t = \infty)/E_r(0) \simeq (1 + 1.6q^2/\sqrt{\epsilon})^{-1}$ is the Rosenbluth-Hinton residual zonal flow [9], $E_r^{neo} = (T_i/e)(\partial \ln N_\alpha/\partial r)$ describes the equilibrium value of the radial electric field which follows the standard neoclassical relationship between E_r and $U_\parallel$ [10], and $\gamma_c \simeq \nu_{ii}$ is the collisional damping rate of the zonal flow [11, 12]. From the discussion above it is clear that the GAM is essentially an ion mode, where the ion polarization current is responding to charge separation caused by radial ion grad-B drifts as delineated in the first two terms of Eq. (3).

3.   4D TEMPEST Simulation Results in Circular Geometry

In this section we will discuss the GAM collisionless damping mechanism, the radial propagation and the "quasi-steady state conditions" on the standard neoclassical transport time scale. We develop a relaxation method to efficiently solve the gyrokinetic Poisson equation to remove the gyrosheath singularity, to correctly yield the standard neoclassical relation between E_r and $U_\parallel$, and simultaneously to obtain the poloidal variation of the electrostatic potential. With the fully nonlinear (full-f) continuum code TEMPEST we compute the radial particle and the heat flux, the evolution of the electric field through different phases of relaxation (development of GAMs, their radial propagation, and their long-time collisional decay) in a circular-geometry edge plasma [2, 4].

3.1   Collisionless damping of Geodesic-Acoustic Modes

In our 4D simulations (with $\partial/\partial\zeta = 0$ in the 5D code) for a homogeneous plasma, the initial ion distribution is a local Maxwellian. The charge is radially separated by an initial sinusoidal perturbation of the ion density with no variation within the flux surfaces $\delta n_i = \delta n_0 \sin(2\pi r/L_\psi)$. The electron model is a fully nonlinear Boltzmann $n_e = \langle n_i(\psi, \theta, t = 0)\rangle \exp(e\phi/T_e)/\langle \exp(e\phi/T_e)\rangle$, where $\langle\rangle$ represents the flux-surface average. This choice of coefficient for the Boltzmann electron model means that there is no cross-field electron transport. Both the radial and poloidal boundary conditions are periodic. We consider a simple circular cross-section tokamak with the magnetic field $\mathbf{B} = B_\zeta \mathbf{e}_\zeta + B_\theta \mathbf{e}_\theta$, where ζ and θ are the toroidal and poloidal angles of a torus, respectively, with $\theta = 0$ chosen to be at the outboard midplane of the torus. The inverse aspect ratio $\epsilon = r/R_0$ where r is the minor radius is not assumed to be small. The major radius is given by $R = R_0(1 + \epsilon\cos\theta)$ and $B_\zeta = B_0 R_0/R$. The equilibrium parameters used are $B_0 = 15$T, $R_0 = 1.71$m, and $T_i = T_e = 3$keV with deuterium ions. We take $B_\zeta(r)$ to be radially uniform to justify the radial periodic boundary conditions. The large B_0 is used for the global simulations with $\delta_i/L_\psi \ll 1$, where $\delta_i = q\rho_i$ is the drift-orbit size and L_ψ is the radial box size. The resolution is $n_\psi = 32, n_\theta = 64, n_E = 30$ and $n_\mu = 60$. $\rho_s = c_s/\Omega_{ci}, c_s = \sqrt{2T_e/M_i}, v_{thi} = \sqrt{2T_i/M_i}, T_e = T_i, \epsilon = r/R = 0.2$. γ_{GAM} and ω_{GAM} are measured in units of v_{thi}/R_0.

The damping rate of the GAM vs q for a fixed $\epsilon = 0.2$ and $k_r\rho_i \simeq 0.1375$ is plotted in

Fig. 1a). The curves come from the theory of Gao et al [7], where a series of Bessel functions for finite orbit width and plasma-dispersion-function-like integrals along the Landau contour for higher-harmonic resonances are included. The dispersion relation is solved by a direct numerical-integration technique retaining many harmonics. The dotted curve omits the finite-orbit-width (FOW) effect; the dot-dashed curve includes additional damping at the 2nd resonance as done by Sugama and Watanabe [6] and Gao et al [7]; the dashed curve is the theory retaining additional damping up to the 4th resonance; the solid curve is the theory retaining additional damping up to the 10th resonance; The black points are TEMPEST simulation results. Also plotted are results from a 5D gyrokinetic continuum code GYRO (purple squares) [13], and a gyrokinetic PIC code XGC (red diamonds) [14]. The error bar from TEMPEST simulations represents the uncertainty in fitting to a single decaying exponential. The FOW effect dramatically enhances the GAM damping rate at $q > 2$ by inducing multiple resonances in phase space. For the same parameters, the damping rate is almost zero if the FOW effect is ignored. Furthermore, Fig. 1a) clearly shows that higher-harmonic resonances at $v_{\parallel}^{res} \simeq \omega_G q R_0 / n$ with $n > 2$ become important when $q > 3.5$. The higher-harmonic resonances are included in the simulations, and comparisons between theory and simulation show that the theory retaining up to the 2nd resonance is a good approximation only for $q < 3.5$. Our theoretical treatment, retaining up to 4th resonance, is required for $3.5 < q < 9$. A corresponding analytical expression for the damping rate is systematically derived, including higher-order harmonics of the ion transit frequency and valid over a broad range $k_r \rho_{it} \ll 1$ and $q \gg 1$ [8]. For the same parameters used in Fig. 1a), the analytical formula predicts damping rates in very good agreement with the numerical and simulation results in its validity regime: $q > (k_r \rho_{it})^{-1/2} \sim 3$.
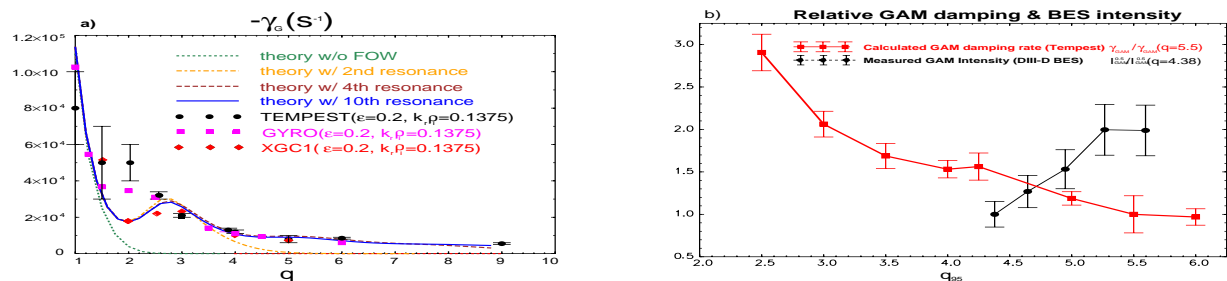

FIG. 1: a) GAM damping rate γ_G vs q for $\epsilon = 0.2$ in homogeneous plasmas. The curves come from Gao et al theory [7] with and without the finite-orbit-width effect, the black points are TEMPEST simulation results, the purple squares are GYRO simulation results, and the red diamonds are XGC simulation results. b) GAM damping rate and integrated GAM amplitude (square-root of intensity I) versus q_{95} within one discharge near $r/a = 0.9$ during the current ramp up (acquired at 100ms intervals) from Ref. [15] in DIII-D edge plasmas. Here $\gamma_{GAM}(q = 5.5) = 3.2 \times 10^3/s$.

3.2   Radial Propagation of Geodesic-Acoustic Modes

TEMPEST simulations were carried out for an inhomogeneous plasma with density and temperature profiles chosen to model the DIII-D edge pedestal: magnetic field $B_t = 1.5T$, $R_0 = 1.71m$, $q = 3$ and $\varepsilon = 0.3$. The ion guiding-center density and temperature profiles are initialized as a hyperbolic tangent (tanh) function of radius centered around the middle of the simulation domain. In this simulation a Lorentz collision model is used. An initial pulse-like perturbation of the ion density is given with the peak centered around the middle of the pedestal. A series of TEMPEST simulations were compared with experimental measure-

ments from a q-scan. The enhanced GAM damping at high q is found again, which is consistent with the experimental measurements of the scaling of the GAM amplitude with edge q_{95} [15]. A simple model for the BES intensity I can be written as $dI/dt = S_{turb} - \gamma_{GAM}(q)I$, where S_{turb} is the source term representing the effects of the "external" forces induced by the small-scale turbulence. If the source S_{turb} is a weak function of q, then for steady-state conditions a strong drop in γ_{GAM} as q increases should correlate with an increase in GAM intensity I, as shown in Fig. 1b). However over that same range of q variation in Fig. 1a) as the BES measurement, there is very little change in the damping rate. The difference may be due to the real DIII-D parameters and particularly the pedestal-like temperature profiles which turn the GAM oscillation into radial propagation in the form of outgoing waves and set the radial scale of the GAM wave-like radial structure in our TEMPEST simulation. This radial scale, in turn, determines the strength of the higher harmonic resonant damping. The enhanced GAM damping may also help to explain the similar q-scaling of the GAM amplitude, observed using Doppler reflectometry in ASDEX Upgrade [16].
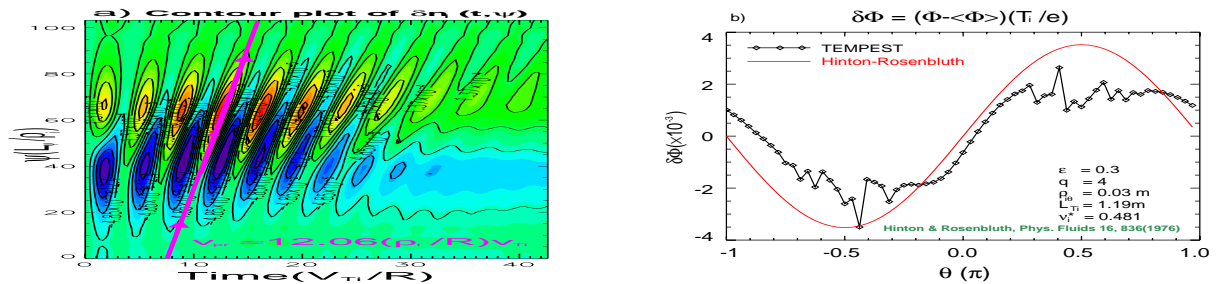

FIG. 2: a) Contour plot of the perturbed ion density $\delta n_i/N_{i0} = (N_i - N_{i0})/N_{i0}$ as a function of radial position and time. Here L_ψ is the radial box size. b) Poloidal variation of potential versus poloidal angle.

TEMPEST simulations show that the kinetic GAMs exist in the edge for steep plasma gradients in the form of outgoing waves [17, 18], as shown in Fig. 3; and the ion temperature inhomogeneity is necessary for GAM radial propagation [2]. The linear relationship of the peak of the contour of the perturbed ion density $\delta n_i/N_{i0}$ as a function of radial position and time indicates that the group velocity and phase velocity are the same. A simple estimate shows that its radial wavelength is a function of the ion temperature gradient scale length $\rho_i^{2/3} L_{Ti}^{1/3}$ [17], and its radial propagation velocity is on the order of the radial ion grad-B drift. From the simple estimate based on a linearly decreased ion temperature profile, we obtain $v_{pr} \propto (\sqrt{7 + 4\tau}/4)f(q)(L_{Ti}/\rho_i)^{1/3}(\rho_i/R)v_{Ti}$ where $f(q) = \sqrt{1 + 46/49q^2}$. The TEMPEST simulations yield the coefficient and the following relationship is obtained $v_{pr} \simeq 0.76(\sqrt{7 + 4\tau}/4)f(q)(L_{Ti}/\rho_i)^{1/3}(\rho_i/R)v_{Ti}$. Here the plasma parameters are evaluated at the radial position where the GAM is excited near the singular layer ($\omega = \omega_{GAM}$), with the well-known Airy function behavior. In this TEMPEST simulation, it is the position with the peak ion temperature gradient where the peak density perturbation is initiated. The experimental BES measurements show a very coherent GAM in DIII-D; it has a well-defined frequency in a given plasma condition/time, along with a well-defined k_r (typically near 1 cm^{-1} at about f=14-16 kHz). It appears to propagate radially outward at the outboard midplane. The measured and calculated radial propagation velocity are $v_{pr}^{DIII-D} \equiv 2\pi f/k_r \simeq (8.79 - 10.00) \times 10^2 \text{m/s}$ and $v_{pr}^{Sim} \simeq 8.69 \times 10^2 \text{m/s}$ with $L_{Ti} \simeq 10\rho_i$ and $\tau = 1$, showing agreement to within 15%. The probe experimental measurements on tokamak HL-2A also show that the localized GAM packet is observed to propagate outward

in the radial direction with nearly the same phase and group velocity, which is consistent with TEMPEST simulations [19]. We note that the measured local velocity may be different from the calculated velocity using above formula because the GAM velocity is determined by the parameters at the location where the GAM is excited, not where it is measured. Therefore, by combining with ion and electron temperature, and q profiles, the measured velocity can be used to determine the location where the GAM is excited.

3.3   Radial electric field of neoclassical plasmas

Traditionally the radial electric field of a neoclassical plasma is evaluated according to the radial Ampere-Maxwell's law averaged over a closed-flux surface as described in Sect. 2. However, this method is incomplete in the sense that the poloidal electric field cannot be solved simultaneously in a consistent way. This is an unsatisfactory situation since the potential varies significantly in the edge plasma around the X-point and in the divertor leg region due to contact with divertor plates. The gyrokinetic Poisson equation is seldom used because the small coefficient in front of the Poisson operator associated with the gyroradius makes the equation nearly singular due to a gyrosheath at radial boundaries when $\rho_s \ll L_P \ll L_B$. Here, $L_P = |\nabla(\ln P)|^{-1}$ is the characteristic gradient scale length for the plasma profile, and $L_B = |\nabla(\ln B)|^{-1}$ the characteristic length for the magnetic field. We develop a relaxation method to efficiently solve the gyrokinetic Poisson equation to remove the singularity and to correctly yield the standard neoclassical relationship between E_r and $U_\parallel$. In a special case with a flat ion temperature profile and Lorentz collisions, TEMPEST simulations show that the electrostatic potential relaxes to a steady state, and a Boltzmann relation is reached [2], $(Z_i e/T_i)\partial\phi/\partial\psi + \partial\ln P_i/\partial\psi = 0$, as expected from the theory for the case of zero temperature gradient [20]. The steady-state $U_\parallel$ is very small due to the specified Maxwellian radial boundary condition with zero flow velocity.

In a general case with an ion temperature gradient, starting from an initial state with $E_r = 0$ and $U_\parallel = 0$, the equilibrium-scale radial electric field is quickly established on the order of a fraction of a collision time after the relaxation of GAM oscillations and zonal flow, and obeys the standard neoclassical relationship between E_r and $U_\parallel$, while $U_\parallel$ is not yet fully evolved. The further development of $U_\parallel$ on the transport time scale requires careful formulation of the gyrokinetic equation and gyrokinetic Poisson equation, including sources and sinks, as well as higher order in ρ_i/L_B corrections to the first-order gyrokinetic equation. Using the relaxation approach to solve the gyrokinetic Poisson equation we are able to obtain the standard neoclassical relationship between E_r and $U_\parallel$ [2], and the first-order (poloidal) correction to the equilibrium-scale radial electric field. The poloidal variation of the potential has been analytically estimated to vary as [21]

$$\left(\frac{Z_i e}{T_i} + \frac{e}{T_e}\right)\delta\Phi \simeq C\epsilon\frac{\rho_{i\theta}}{\sqrt{2}L_{Ti}}\sin\theta. \qquad \delta\Phi = (\Phi - \langle\Phi\rangle) \qquad (5)$$

where $\rho_{i\theta}$ is the ion gyro-radius at the poloidal magnetic field, and C is a coefficient: $C \simeq 1.81\nu_{*i}$ in the banana regime and $C \simeq \sqrt{2}/2$ in the plateau regime, where $\nu_{*i} = \epsilon^{-3/2}\nu_{ii}\sqrt{2}qR_0/v_{Ti}$. The comparison of the poloidal variation of potential is shown in Fig. 2b) for the analytical estimate and the TEMPEST simulation, which is in qualitative agreement with analytical predictions from Eq. (5) that $\delta\Phi(\psi,\theta)$ is found to vary sinusoidally with a magnitude lower than the Hinton-Rosenbluth prediction. A similar trend is found in a newly developed Eulerian code NEO for numerical studies of neoclassical transport [22].

The lack of a quantitative agreement is possibly due to the following [22]: (1) for the banana-regime prediction the Hinton-Rosenbluth derivation develops a singular component due to inadequate treatment of the trapped/passing particle boundary layer and thus only the Fourier sine coefficient, which is finite, is reported in the final analytical result. (2) the finite ϵ effects are neglected in the analytical theory.

4.   4D TEMPEST Simulation of Plasmas flows in divertor geometry

Additional results are obtained with 4D TEMPEST simulations of plasma transport in single-null tokamak geometry. One set of simulations studies the effect of high-energy drift orbits from the pedestal region that can extend across the separatrix into the scrape-off layer (SOL). The sign of the ion parallel velocity determines if the drift orbit is radially inward or outward. Near the outer midplane this kinetic effect results in substantial mean ion flow of the hot ions toward the inner divertor plate for the ion gradient-B drift toward the X-point. For DIII-D H-mode discharge 96333, we simulate this effect by taking the ion distribution boundary condition at the top of the pedestal to be a 1 keV Maxwellian with density of $5 \times 10^{19} m^{-3}$, and then allow TEMPEST to evolve the distribution to the separatrix and into the SOL. An energy-dependent Lorentz collision operator is used. In the outer-midplane SOL, the ion distribution function shows a pronounced high-energy tail giving a mean parallel velocity near sonic values toward the inner divertor, and this mean flow reverses sign at the inner midplane as expected; coupling of this flow to the colder SOL plasma needs to be modeled. Figure 3a shows the outer midplane profiles of ion density and temperature for this case. In addition, the kinetic simulation shows that the flux of ions lost at the divertor plates is nearly as large on the private-flux side of the separatrix as on the SOL side. Inclusion of a 1 kV electrostatic potential that peaks on the separatrix and decays to zero at each radial boundary (core interface, private-flux wall, and SOL wall) results in a radial shift of the plasma (and thus hot-ion flux) toward the private-flux side on the outer divertor and toward the SOL side on the inner divertor as shown in Fig. 3b.
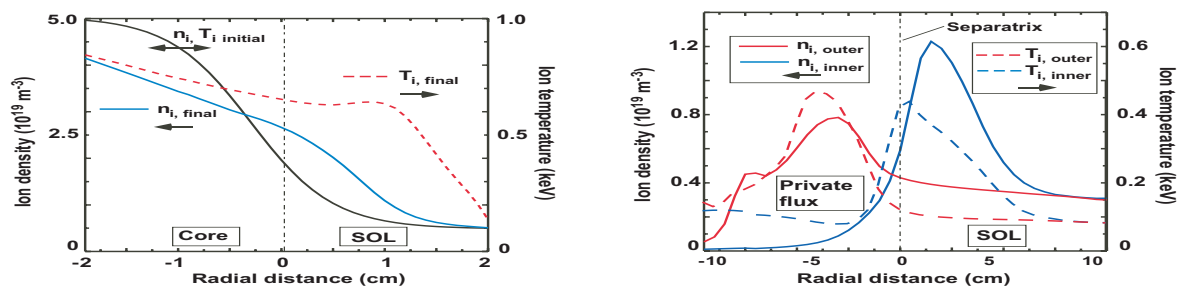

FIG. 3: a) Radial profiles of ion density and temperature for TEMPEST simulation of DIII-D single-null divertor; b) Final profiles of ion density and temperature at the inner and outer divertor plates for the case with 1 kV potential.

5.   Summary

The newly discovered higher harmonic resonances significantly enhance GAM damping at high-q ($n > 2$), are necessary to explain the damping observed in q-scans of our gyrokinetic simulations, and consistent with the experimental measurements of the scaling of the GAM amplitude with edge q. The kinetic GAM exists in the edge for steep plasma gradients in

the form of radially outgoing waves as experimentally measured, and the ion temperature inhomogeneity is necessary for GAM radial propagation. The radial propagation velocity in simulation agrees with theoretical estimates and experiments.

Acknowledgments

References

[1] X. Q. Xu, Z. Xiong, M. R. Dorr, J. A. Hittinger, *et al.*, *Nucl. Fusion* **47**, 809 (2007).

[2] X. Q. Xu, *Phys. Rev. E.* **78**, 016406 (2008).

[3] N. Winsor, J. L. Johnson, J. M. Dawson Phys. Fluids, **11**, 2448 (1968).

[4] X. Q. Xu, Z. Xiong, Z. Gao, W. M. Nevins, *et al.*, Phys. Rev. Lett. **100**, 215001 (2008).

[5] V. B. Lebedev, P. N. Yushmanov, P. H. Diamond, *et al.*, *Phys. Plasmas* **3**, 3023 (1996).

[6] H. Sugama and T. -H. Watanabe, J. Plasma Phys. **72**, 825 (2006).

[7] Zhe Gao,K. Itoh, H. Sanuki, and J. Q. Dong, *Phys. Plasmas* **15**, 072511 (2008)

[8] Z. Y. Qiu, L. Liu, and F. Zonca, submitted to Plasma Phys. Control. Fusion, 2008.

[9] M. N. Rosenbluth and F. L. Hinton, Phys. Rev. Lett. **80**, 724 (1998).

[10] F. L. Hinton and R. D. Hazeltine, *Rev. Mod. Phys.* **48**, 239 (1976).

[11] F. L. Hinton and M. N. Rosenbluth, *Plasma Phys. Control. Fusion* **41**, A653 (1999).

[12] Y. Xiao and P. J. Catto, *Phys. Plasmas* **14**, 055910(2007).

[13] J. Candy, R. E. Waltz, Journal of Computational Physics 186 (2003) 545-581.

[14] S. Ku, C. S Chang, M. Adams, et al.,*J. Phys.*, **46** 87-91(2006).

[15] G. R. Mckee *et al.*, Plasma Phys. Control. Fusion **48**, s123 (2006).

[16] G. D. Conway, *et al.*, Plasma Phys. Control. Fusion **50**, 085005 (2008).

[17] K. Itoh, et al, Plasma Fusion Res. **1**, 037 (2006).

[18] F. Zonca and L. Chen, *Euro. Phy. Lett.* **83** 35001 (2008).

[19] T. Lan, A. D. Liu, C. X. Yu,*et al.*, *Phys. Plasmas* **15**, 056105 (2008)

[20] M. N. Rosenbluth, *et al.*, in *Plasma Physics and Controlled Nuclear Fusion Research, 1970 (International Atomic Energy Agency, Vienna, 1971)*, Vol. **1**, p. 495.

[21] F. L. Hinton and M. N. Rosenbluth, *Phys. Fluids* **16**, 836 (1973).

[22] E. A. Belli and J.Candy, Plasma Phys. Control. Fusion 50 (2008) 095010.